A wave-equation splitting algorithm for modeling and migration in anisotropic media

Ricardo A.R.Fernandes * and Irshad R. Mufti
PETROBRAS - E & P and Inst. of Geophysics, Federal University of Bahia - Brazil

Abstract

The interpretation of seismic data acquired in areas characterized by velocity anisotropy is of particular interest in reservoir geophysics. Foward modeling and adequate seismic migration algorithms can enhance the dependability of interpretation. We attack this problem by exploiting the most fundamental property of the anisotropic media which makes them different from the isotropic media, viz., the variation of velocity with direction. This is accomplished by splitting the wave equation and replacing it by two or more simpler equations which involve only one spatial derivative but a different velocity in each case. The evaluation of the wavefield is carried out by setting up a finite-difference model in which a set of difference relations derived from the simpler equations is used in an alternate fashion. We present two examples of application, one in 2D and another in 3D.

Introduction

The current methods of imaging in areas with anisotropy do not, in general, yield satisfactory results . Forward modeling and a proper migration algorithm can be very helpful in enhancing the dependability of interpretation (Igel et alli, 1995 and Dong and McMehan, 1991). We put forward a new method for evaluating the wavefield in the presence of velocity anisotropy. It exploits the most fundamental property of the anisotropic media which makes them different from the isotropic media, viz., the variation of velocity with direction. We accomplish our objective by developing an accurate finite-difference computational scheme in which the wavefield is computed separately for each direction by using a different velocity. This involves splitting the wave equation and replacing it by two or more simpler equations which are mathematically equivalent to the original equation but include only one spatial derivative. Since such an approach depends neither on the spatial dimensions of the problem nor on a particular version of the wave equation, it offers a broad range of applications for solving a variety of geophysical problems related to imaging. However we shall restrict our treatment to the acoustic wave equation.

The new algorithm

It would be convenient to start the following treatment with the acoustic wave equation in three dimensions; it can be expressed as

$$\begin{aligned} u_{xx} + u_{yy} + u_{zz} &= \frac{1}{c^2} u_{tt} \\ &+ f(t)\delta(x - x_s)\delta(y - y_s)\delta(z - z_s) \end{aligned} \tag{1}$$

where $u(x, y, z, t)$ is the wavefield, $c(x, y, z)$ is the velocity of the medium, $f(t)$ is a band-limited line source located at (x_s, y_s, z_s), x, y represents ground level and z is depth.
In finite-difference modeling, the propagation of the wavefield can be computed by replacing equation 1 by:

$$\begin{aligned} u^{n+1}_{i,j,k} &= g_{i,j,k}[u^n_{i+2,j,k} + u^n_{i-2,j,k} + u^n_{i,j+2,k} \\ &+ u^n_{i,j-2,k} + u^n_{i,j,k-2} + u^n_{i,j,k+2} \\ &- 16\left(u^n_{i-1,j,k} + u^n_{i+1,j,k} + u^n_{i,j-1,k} + u^n_{i,j+1,k}\right. \\ &+ \left. u^n_{i,j,k-1} + u^n_{i,j,k+1}\right) \\ &+ 90u^n_{i,j,k}] + 2u^n_{i,j,k} - u^{n-1}_{i,j,k} \end{aligned} \tag{2}$$

where

$$g_{i,j,k} = -\left[\frac{\left(c_{i,j,k} \times \frac{\Delta t}{h}\right)^2}{12}\right] \tag{3}$$

Relation 2 is fourth-order accurate in space and second-order accurate in time. h indicates the grid spacing assumed to be uniform both for the lateral and vertical directions and Δt represents the time step for computing the wavefield. The discrete indices i, j, k and n correspond to x, y, z and t respectively. In equation 2 the source term is implied but is being omitted for notational simplicity.

Instead of basing our treatment on equation 1, we can obtain essentially the same results by splitting this equation into two components and using them in an alternate fashion (Mufti, 1985). Thus we can use the following equations:

$$u_{xx} = \frac{1}{3}\left[\frac{1}{c^2}u_{tt} + f(t)\delta(x-x_s)\,\delta(y-y_s)\,\delta(z-z_s)\right] \quad (4)$$

$$u_{yy} = \frac{1}{3}\left[\frac{1}{c^2}u_{tt} + f(t)\,\delta(x-x_s)\,\delta(y-y_s)\,\delta(z-z_s)\right] \quad (5)$$

$$u_{zz} = \frac{1}{3}\left[\frac{1}{c^2}u_{tt} + f(t)\,\delta(x-x_s)\,\delta(y-y_s)\,\delta(z-z_s)\right] \quad (6)$$

The alternate use of these equations accompanies evaluating the wavefield at one-third time steps ($\Delta t/3$). One could argue that no significant advantage is to be gained by splitting the wave equation. It is worth mentioning here that equation 2 depends on three spatial variables, but equations 4, 5 and 6 involve only one spatial variable. We can exploit this fact for computing the wavefield in the presence of velocity anisotropy by assigning different velocities to these equations. Thus if the medium under consideration has any anisotropy such that:

$$c_x \neq c_y \neq c_v$$

where c_x and c_y are the velocities in each of the horizontal directions and c_v is the velocity in the vertical direction, equations 4, 5 and 6 will take the form:

$$\begin{aligned} u_{i,j,k}^{n+\frac{1}{3}} &= -\frac{1}{36}\left(\frac{c_{v_{i,j,k}}\Delta t}{h}\right)^2\Big[u_{i,j,k-2}^{n} + u_{i,j,k+2}^{n} \\ &- 16\left(u_{i,j,k-1}^{n} + u_{i,j,k+1}^{n}\right) + 30u_{i,j,k}^{n}\Big] \\ &+ 2u_{i,j,k}^{n} - u_{i,j,k}^{n-\frac{1}{3}} \end{aligned} \quad (7)$$

$$\begin{aligned} u_{i,j,k}^{n+\frac{2}{3}} &= -\frac{1}{36}\left(\frac{c_{y_{i,j,k}}\Delta t}{h}\right)^2\Big[u_{i,j-2,k}^{n+\frac{1}{3}} + u_{i,j+2,k}^{n+\frac{1}{3}} \\ &- 16\left(u_{i,j-1,k}^{n+\frac{1}{3}} + u_{i,j+1,k}^{n+\frac{1}{3}}\right) + 30u_{i,j,k}^{n+\frac{1}{3}}\Big] \\ &+ 2u_{i,j,k}^{n+\frac{1}{3}} - u_{i,j,k}^{n} \end{aligned} \quad (8)$$

$$\begin{aligned} u_{i,j,k}^{n+1} &= -\frac{1}{36}\left(\frac{c_{x_{i,j,k}}\Delta t}{h}\right)^2\Big[u_{i-2,j,k}^{n+\frac{2}{3}} + u_{i+2,j,k}^{n+\frac{2}{3}} \\ &- 16\left(u_{i-1,j,k}^{n+\frac{2}{3}} + u_{i+1,j,k}^{n+\frac{2}{3}}\right) + 30u_{i,j,k}^{n+\frac{2}{3}}\Big] \\ &+ 2u_{i,k}^{n+\frac{2}{3}} - u_{i,k}^{n+\frac{1}{3}} \end{aligned} \quad (9)$$

The indices n, $n+\frac{1}{3}$, $n+\frac{2}{3}$, $n+1$, $\cdots$ imply the one-third time steps $n\Delta t$, $(n+\frac{1}{3})\Delta t$, $(n+\frac{2}{3})\Delta t$, $(n+1)\Delta t$, $\cdots$. Since we are considering a 3-D problem, the procedure described above will be suitable to media possessing arbitrary anisotropy. Reduction of this algorithm to 2-D is straightforward but it will apply only to transversely isotropic media.

We have developed a reverse-time migration algorithm based on the same splitting scheme for 2D and 3D anisotropic media. For the reverse-time migration we must excite the model at its surface boundary by using each trace of the unmigrated data as source function. All traces are fed into the model simultaneously in the reverse order of time and the splitting algorithm performs the propagation until the trace length has been used up. The final configuration of the wavefield is the depth-migrated image of the subsurface.

Applications

We shall consider two examples of application. The first one is based on Model 1 shown in Figure 1. All layers in this model are isotropic except the first layer (vertical velocity of 2740 m/s and a horizontal velocity of 3290

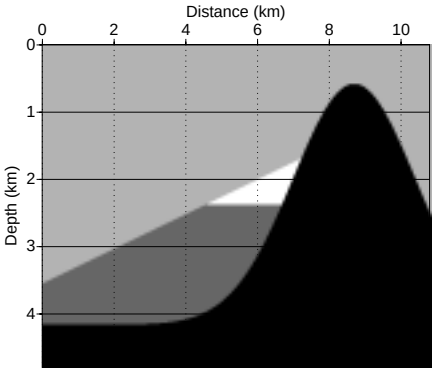

Figure 1: Geologic Model 1.

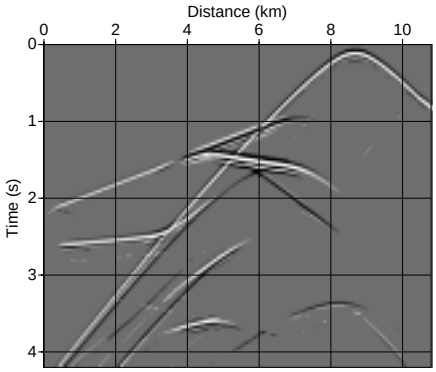

Figure 2: Seismic section based on Model 1, with anisotropy in the first layer.

m/s). We used the concept of the exploding reflector to compute a seismic section for this structure. The results are shown in Figure 2. As expected, the influence of anisotropy is more pronounced on those events which originate from steeply dipping reflectors. The depth-migrated section is shown in figure 3. The splitting algorithm provides the proper tool for seismic imaging.
The second example is based on Model 2 (figure 4) which represents a vertical fault and a dipping layer in y direction. Velocities are 1500 m/s in the upper layer, 2500 m/s in the intermediate layer and 4000 m/s in the lower one. Figures 5 and 7 show the zero-offset sections obtained with the splitting algorithm, respectively, at $x = 150$ meters and at $y = 200$ meters. Migrated sections through the data volume at the same x and y coordinates of the zero-offset sections (figures 5 and 7), show that our algorithm can adequately handle any geologic event actually present in the subsurface.

Conclusions

We have presented a new algorithm for wavefield evaluation which seems to be ideally suited for imaging in areas with anisotropic subsurface structures. Its development was motivated by the idea that such problems could be handled more conveniently and in a natural way if we try to do the same to the wave equation what anisotropy does to the earth. We accomplished this objective by splitting the multi-dimensional equation into two or more one-dimensional equations and assigning a different velocity to each of them as dictated by the anisotropic characteristics of the earth.

References

Dong, Zhengxin and McMechan, G.A., 1991 - Numerical modeling of seismic waves with a 3-D anisotropic scalar-wave equation. Bulletin of the Seismological Society of America, vol 81, pages 769-780.

Ebrom, D. and Sheriff, R.E., 1992 - Anisotropy and reservoir development, Reservoir Geophysics, SEG, pages 355 -361.

Igel, H., Mora, P. and Riollet, B , 1995 - Anisotropic wave propagation through finite-difference grids. Geophysics, vol. 60, pages 1203-1216.

Mufti, I.R., 1985 - Seismic modeling in the implicit mode. Geophysical Prospecting, vol. 33, pages 619 - 656.

Acknowledgements

The authors are grateful to PETROBRAS and CNPq (The Brazilian National Science Foundation) for financially supporting this research.

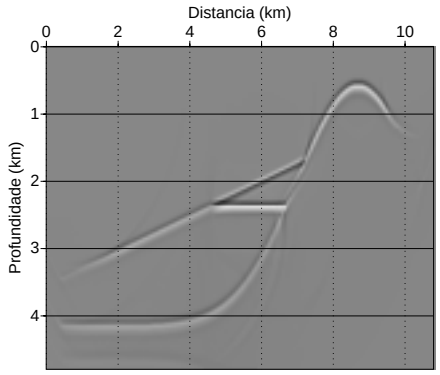

Figure 3: Migrated section for the anisotropic case, using the splitting algorithm.

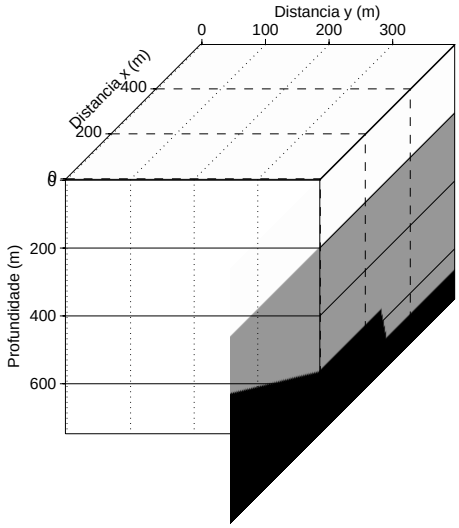

Figure 4: Geologic Model 2.

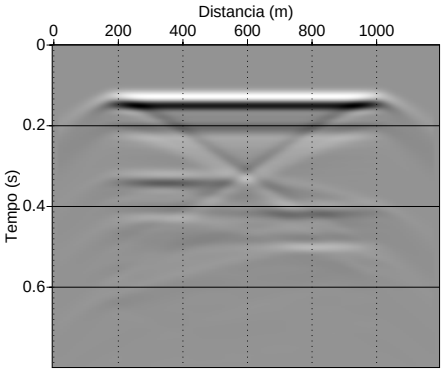

Figure 5: Seismic cross-section of Model 2, at coordinate $y = 200$ meters, obtained with a three step modeling algorithm in 3-D.

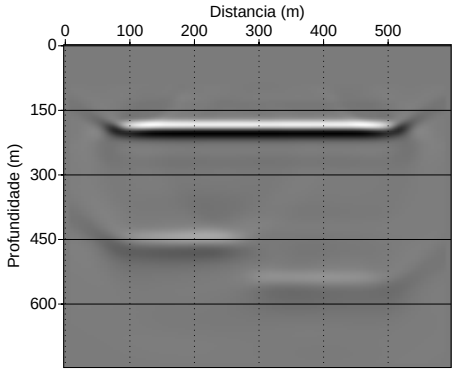

Figure 6: 2D Migrated cross-section of Model 2, at coordinate $y = 200$ meters obtained with the splitting reverse-time migration algorithm.

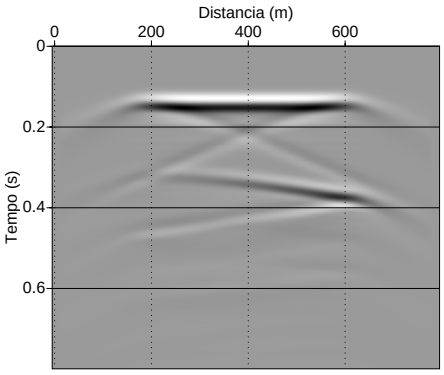

Figure 7: Seismic cross-section of Model 2, at coordinate $x = 150$ meters.

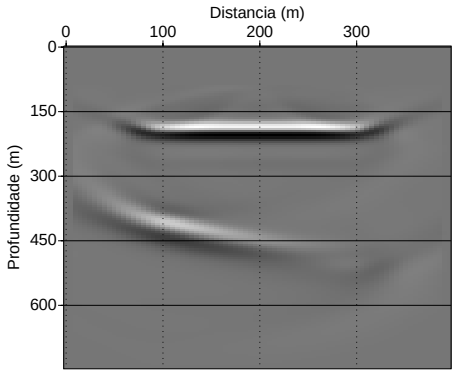

Figure 8: 2D Migrated cross-section of Model 2, at coordinate $x = 150$ meters obtained with the splitting reverse-time migration algorithm.